Journal of Manufacturing Processes
Vol. 1/No. 1
1999

# Striation Formation and Melt Removal in the Laser Cutting Process

**Kai Chen** and **Y. Lawrence Yao**, Dept. of Mechanical Engineering, Columbia University, New York, New York

## Abstract

The mechanisms of melt ejection and striation formation in continuous wave laser cutting of mild steel are discussed. Melt ejection from the cutting front is shown to be a cyclic phenomenon. Striation formation is strongly affected by the oscillatory characteristic of the thin liquid film on the cutting front during melt ejection, together with the oxidation and heat transfer process. Cutting speed determines whether the liquid film will rupture or generate waves on the cutting front. Theoretical explanations are given according to the instability theory of a thin liquid film in a high-velocity gas jet and the diffusion-controlled oxidation theory. Striation frequency and depth are predicted according to the above theories. Experimental investigations were carried out and the results are consistent with the calculations. The better understanding has shed light on further investigations and optimal process development.

***Keywords:*** *Laser Cutting, Striation Formation, Oxidation, Instability*

## Nomenclature

$A$ constant ($m^2/s$)
$B$ constant ($m^2/mol$)
$b$ kerf width (m)
$C$ oxygen concentration ($mol/m^3$)
$c$ wave velocity (m/s)
$c_f$ friction factor
$c_p$ heat capacity (J/(kgK))
$D$ diffusion coefficient ($m^2/s$)
$d$ workpiece thickness (m)
$f$ wave frequency ($s^{-1}$)
$h$ liquid film thickness (m)
$I$ defined in Eq. (11)
$J$ particle current in oxidation ($mol/(m^2s)$)
$K$ heat conductivity (J/(smK))
$k$ wave number ($m^{-1}$)
$k_B$ Boltzmann constant (J/K)
$P_r$ normal stress parameter
$P$ pressure (Pa)
$p_o$ oxygen pressure at interface (Pa)
$R$ Reynolds number of liquid, $R= Vh/\nu$
$s_m$ maximum thickness of oxide layer (m)
$T_i$ tangential stress parameter
$T_0$ activation temperature (K)
$t$ time (s)
$t_p$ time period per oxidation cycle (s)
$U$ gas velocity profile (m/s)
$U_0$ streamwise gas velocity (m/s)
$V$ interfacial velocity (m/s)
$u$ liquid velocity in $x$ direction (m/s)
$v$ liquid velocity in $y$ direction or cutting speed (m/s)
$v_*$ friction velocity (m/s)
$W$ activation energy (J)
$w$ internal energy (J)
$x$ direction along interface
$y$ direction perpendicular to interface
$\alpha$ $\alpha = kh$, dimensionless wave number
$\beta$ defined in Eq. (20)
$\delta$ initial disturbance (m)
$\gamma$ surface tension ($kg/s^2$)
$\lambda$ wave length (m)
$\mu$ viscosity of melt (kg/(ms))
$\mu_g$ viscosity of gas (kg/(ms))
$\rho$ density of melt ($kg/m^3$)
$\rho_g$ density of gas ($kg/m^3$)
$\sigma_{xy}$ tangential perturbation stress (Pa)
$\sigma_{yy}$ normal perturbation stress (Pa)
$\tau$ mean shear stress (Pa)
$\nu$ kinematic viscosity of melt ($m^2/s$)
$\nu_g$ kinematic viscosity of gas ($m^2/s$)
$\psi$ stream function
$\phi$ function in Eq. (3)
$\eta$ disturbance (m)

*Subscripts*

| | |
|---|---|
| upper bar | mean value |
| prime | perturbation value |
| $o$ | interface of oxide and oxygen |
| $s$ | interface of metal and oxide |

## Introduction

The formation of periodic patterns (striation) has drawn much attention in continuous wave laser cut-

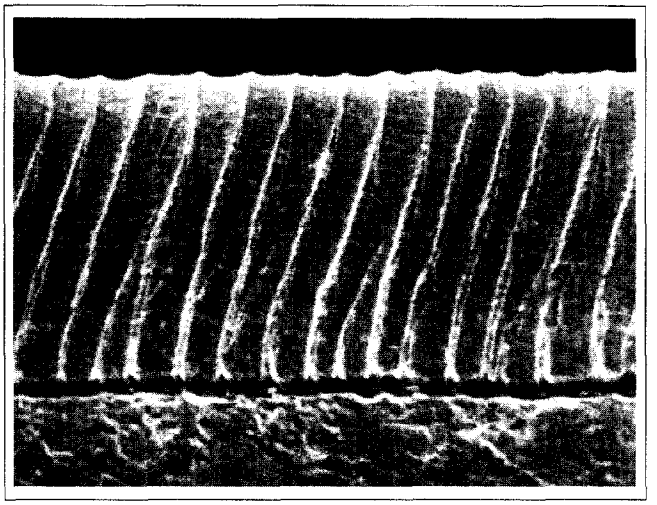

*Figure 1*
**Typical Cut Edge Showing Striation Pattern in Thin Sections**

ting of mild steel because it strongly affects the quality of the finished cut (*Figure 1*). However, the physical mechanisms of striation formation are not fully understood and are far from being quantitatively described. Obviously, striation results from some periodic nature of the cutting process. Most investigators argue that striation patterns are due to an oscillated molten front in the course of laser cutting. There are several possible mechanisms that will result in an oscillated molten front even when optical and mechanical conditions are well controlled. The fluctuation of absorbed laser power during laser cutting and the gas flow interacting with the workpiece will bring about fluctuation of the molten front.[1] In special cases, the liquid layer can oscillate with a natural frequency even without fluctuations in absorbed power.[1] The high-speed gas jet during melt ejection will cause hydrodynamic instabilities of the molten front.[2] Arata et al. for the first time conducted a detailed experimental investigation about the molten front in the cutting process.[3] They suggested that when the cutting speeds are less than the velocity of the reactive front, the ignition and extinction cycles of reaction begin to take place, and they proposed a critical cutting speed of 2 m/min for mild steel of certain thickness, above which no such cycle exists. But some reports indicate even if the cutting speed is above the critical speed, stria still exist.[4,5] A cyclic oxidation model is further suggested.[4] It is explained that, for diffusion-controlled reaction, the rate of chemical reaction is time dependent, being rapid in the early stages but decreasing markedly as the thickness of the oxide layer increases. So the

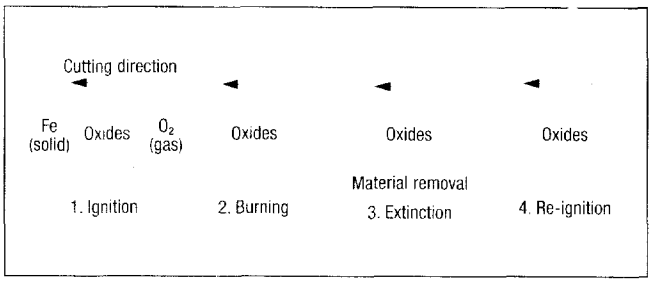


*Figure 2*
**Oxidation Model Proposed by Ivarson et al.[4]**

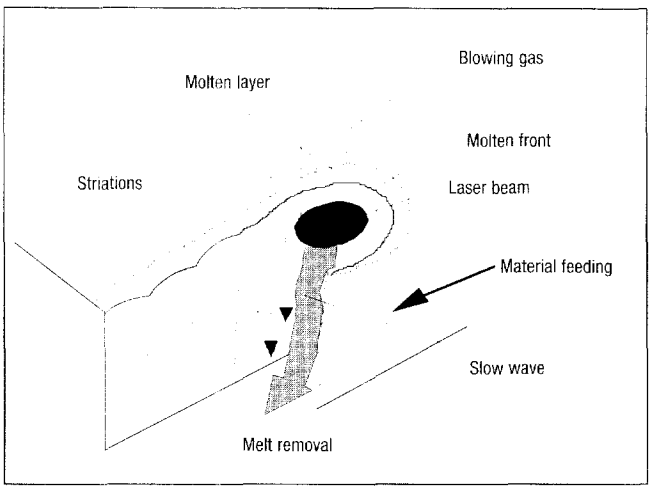


*Figure 3*
**Schematic of Oxygen Cutting of Mild Steel**

oxide layer will expand rapidly at first but slow down afterward. Once the oxide is blown out from the cutting front, due to a sudden decrease of the oxide layer, another expansion will begin (*Figure 2*). Although this model gives a quite convincing explanation on the expansion of the oxide layer, it does not clearly explain how the oxide layer is suddenly reduced. Assuming that the melt removal is a continuous process, the oxidation cycle will not generate striation because when the oxidation and melting speed are finally the same as the melt removal rate, the entire process will no longer be cyclic. The mechanism of melt removal is investigated in this paper, and it is shown that there are cyclic characteristics in the removal process. A schematic of laser cutting of mild steel is shown in *Figure 3*.

## Physical Model of Melt Removal and Striation Formation

The behavior of a thin liquid film under gas flow has been studied over several decades.[6,7] The behavior of the liquid film is largely dependent on the gas velocity, liquid flow rate (or Reynolds number), and

film thickness. Ripples are generated on the surface when a high-velocity gas flows above a thick liquid layer because the viscous dissipation is less than the energy transferred by the wave-induced pressure perturbation. The wave behavior depends on the gas velocity and liquid flow rate. As the film thickness is reduced, the surface smooths out because the friction in the liquid phase can overcome the pressure perturbation. As the film thickness is further reduced to a very small value, it is found that the liquid film becomes unstable because the wave-induced shear stress perturbation is sufficient to overcome the restoring forces, and so-called slow waves are generated on the surface.[8] It is perceivable that, if the liquid film gets even thinner and has a lower fluid flow rate, the film will rupture. In addition to the aforementioned destabilizing forces, the intermolecular dispersion forces may become important in film rupture.[9]

For the case of laser cutting of mild steel, it is commonly accepted that the molten front thickness is of the order of $10^{-5}$ m.[2,3,10] In such an order of thickness, the molten front is unstable and can easily rupture.

Consider the top part of the molten front (*Figure 4*). At low cutting speeds, the liquid film has relatively long exposure time in the gas flow, and the liquid film will usually rupture because there is not enough liquid flow rate on the top part of the molten front. This phenomenon has been observed and described by Arata et al.[3] When the cutting speed increases, the period of film rupture becomes shorter. At some critical cutting speed, there is not enough time for instabilities to develop to cause film rupture, and there is always a liquid film on the top of the molten front. This was described by Arata et al.[3] as "steady cutting," which corresponds to a cutting speed above 2 m/min. This thin liquid film for mild steel of certain thickness, however, may still be unstable, and instead of film rupture, slow waves may be generated (it is shown later that the thickness of the liquid film is below the critical thickness under which slow waves are generated). Once the crest of the slow wave moves downward from the top of the molten front, much more melt is removed, and oxidation coupled with heat conduction begins to expand. The process is fast at first and slows down until another wave crest comes and moves the melt downward. Thus, an expansion-compression cyclic pattern is still formed above the so-called critical cutting speed.

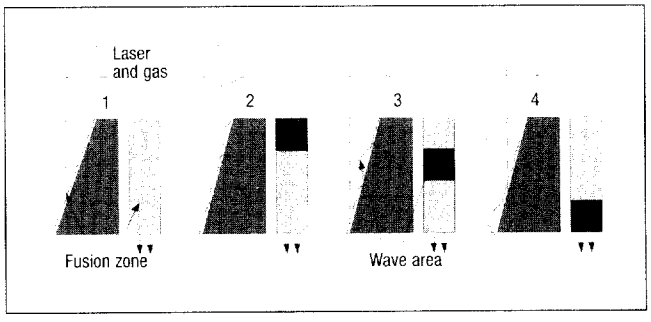


*Figure 4*
**Schematic of Molten Front Change at High Cutting Speeds**

It has been shown by Makashev[10] that a steady flow of the melt layer on the upper edge is impossible. Instead of wave generation, he proposed that a melt drop will quickly grow up to a critical size and then move down. Makashev's theory of droplet formation on the upper edge is not convincing enough because the liquid flow rate is very small and the liquid layer is basically in laminar state (it is estimated that the liquid Reynolds number is comparable to 1). Moreover, as mentioned earlier, there is not enough time for film rupture when the cutting speed is high. Vicanek et al.[2] treated the melt flow as a two-dimensional boundary layer and gave the stationary thickness of the molten layer along with an instability analysis. The stress perturbation, however, was not considered in their approach, and hence the results are not accurate enough to give a quantitative description of the striation pattern.

Melting (or oxidation) and melt ejection are essentially coupled with each other to form a cyclic pattern at the molten front. Because of the wave formation at the molten front, the melt ejection shows a cyclic nature that causes the oxide layer to oscillate and brings about the oscillation of oxidation due to high resistance of the oxide layer. Such a process will be explored in more detail in the following sections. Based on the aforementioned explanation, it is obvious that the oscillation frequency of the molten front is related with the wave frequency on the molten front, which is dependent on the momentum and energy balance of the gas flow and the liquid phase.

## Theoretical Background

### Mathematical Formulation

The analysis of the instabilities generated on a liquid film by an adjacent high-speed gas jet begins with the linearized Navier-Stokes equations of the liquid film. Only two-dimensional harmonic distur-

bances are considered here. The two-dimensional treatment will reveal the basic nature of the problem because every periodic three-dimensional disturbance may be represented in terms of a corresponding two-dimensional problem.[11] Suppose the components of velocity, $u_i$, and pressure, $P$, can be written as the sum of mean values $\overline{u_i}$ and $\overline{P}$ and small perturbation values $u_i'$ and $P'$, as follows:

$$u_i = \overline{u}_i + u_i'; \quad P = \overline{P} + P' \tag{1}$$

where subscript $i$ can be in the $x$ or $y$ direction (*Figure 5*), and the velocity will be $u$ or $v$ accordingly.

The linearized equations of motion in a two-dimensional plane can be obtained by canceling the time-independent solution when the above variables are substituted into Navier-Stokes equations, that is:

$$\frac{\partial u_i'}{\partial t} + \overline{u_j}\frac{\partial u_i'}{\partial x_j} + u_j'\frac{\partial \overline{u_i}}{\partial y_j} = -\frac{1}{\rho}\frac{\partial P'}{\partial x_i} + \nu\Delta u_i' \tag{2}$$

where $\rho$ is the density, $\nu=\mu/\rho$ is the kinematic viscosity, and $\Delta$ is the Laplace operator.

The stream function representing a single oscillation of the disturbance, $\eta$, is assumed to be proportional to the disturbance to satisfy the following continuity equation:

$$\psi(x, y, t) = -\phi(y)\eta(x, t) \tag{3}$$

where $\phi$ is a function of $y$.

The sinusoidal disturbance, $\eta$, has the form of (refer to *Figure 5*)

$$\eta = \delta e^{ik(x-ct)} \tag{4}$$

where $\delta$ is the initial disturbance of a small value, $k$ is the wave number, $\lambda = 2\pi/k$ is the wave length, and $c$ is the wave velocity, which may be complex. The perturbation velocities can be written as the derivatives of the stream function, as follows:

$$u' = \frac{\partial \psi}{\partial y} = -\frac{d\phi}{dy}\eta \qquad v' = -\frac{\partial \psi}{\partial x} = ik\phi\eta \tag{5}$$

Substituting them into Eq. (2), taking proper derivatives of each equation, and making subtraction

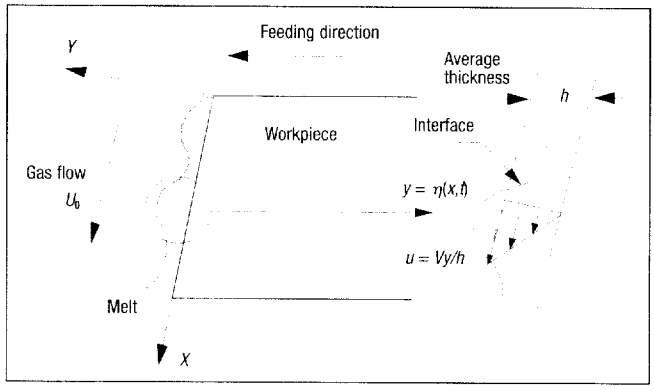


***Figure 5***
**Schematic of Shear Flow and Surface Disturbances**

to cancel out the pressure term will lead to the so-called Orr-Sommerfeld equation, as follows:

$$\nu\frac{d^4\phi}{dy^4} - \left[ik(\overline{u} - c) + 2\nu k^2\right]\frac{d^2\phi}{dy^2} + \left[ik^3(\overline{u} - c) + \nu k^4\right]\phi = 0 \tag{6}$$

The above equations have to satisfy the linearized kinematic and dynamic boundary conditions as well as the condition of vanishing perturbation velocity at the wall. The linearized kinematic condition at the liquid surface is as follows:

$$v' = \frac{\partial \eta}{\partial t} + V\frac{\partial \eta}{\partial x}, \text{ at } y = h \tag{7}$$

where $h$ is the thickness of the liquid film and $V$ is the interface velocity.

The dynamic conditions require the continuity of the tangential perturbation stress, $\sigma_{xy}$, at the interface, that is:

$$\mu\left(\frac{\partial u'}{\partial y} + \frac{\partial v'}{\partial x}\right) = \sigma_{xy}, \text{ at } y = h \tag{8}$$

and the equilibrium of the resisting forces and the normal perturbation stress, $\sigma_{yy}$ (gravity is neglected),

$$-P' + 2\mu\frac{\partial v'}{\partial y} = \gamma\frac{\partial^2 \eta}{\partial x^2} + \sigma_{yy}, \text{ at } y = h \tag{9}$$

where $\gamma$ is the surface tension.

When written in the form of $\phi$ [refer to Eq. (5)], Eqs. (7), (8), and (9) become

$$\phi = V - c, \text{ at } y = h \tag{10}$$

$$\frac{d^2\phi}{dy^2} + k^2\phi + (\mu\eta)^{-1}\sigma_{xy} = 0, \text{ at } y = h \tag{11}$$

$$(ik)^{-1}\nu\frac{d^3\phi}{dy^3} + \left[(c - V) + 3ik\nu\right]\frac{d\phi}{dy} + V\phi/h + k^2\gamma/\rho - (\rho\eta)^{-1}\sigma_{yy} = 0, \text{ at } y = h \tag{12}$$

In deriving the above results, it is assumed that the liquid velocity has a linear profile $u = Vy/h$ and that the mean shear stress is $\tau = \mu V/h$. The vanishing perturbation velocity at the wall leads to the conditions of

$$\phi = \frac{d\phi}{dy} = 0, \text{ at } y = 0 \tag{13}$$

The instability analysis is basically to solve an eigenvalue problem of Orr-Sommerfeld Eq. (6) with the boundary conditions of Eqs. (10), (11), (12), and (13). The process of solving these equations is left out in this paper; only relevant results are provided. A similar analysis was done by Craik.[8]

It should be pointed out that the wave velocity consists of a real part and an imaginary part: $c = c_r + ic_i$, in which $c_i$ represents the growth of the disturbance and $c_r$ denotes the traveling speed of the wave. Thus, instability occurs when $c_i$ has a positive value. For neutrally stable disturbances ($c_i = 0$), the analysis gives the following results:

$$P_r + \frac{3T_i}{2kh} = \gamma k^2 h \tag{14}$$

$$c_r = V \tag{15}$$

where $P_r$ and $T_i$ are stress parameters such that $\sigma_{yy} = P_r\eta$ and $\sigma_{xy} = T_i\eta$. The condition for Eqs. (14) and (15) to be valid is that $(kh)R$ is small enough. $R$ is the liquid Reynolds number.

$$R = Vh/\nu \tag{16}$$

It is obvious that the two terms on the left side of Eq. (14) represent the surface stress, and the term on the right side is the restoring force of surface tension.

## Instabilities of the Cutting Front

Instability occurs when the surface stress is sufficiently large to overcome the restoring forces of surface tension, that is:

$$P_r + \frac{3T_i}{2kh} \geq \gamma k^2 h \tag{17}$$

For the case of laser cutting, the condition that $(kh)R$ is small is satisfied. When the liquid film is so thin that the intermolecular interaction becomes important, the effect can be included by taking it into a dispersion force term on the left side of the equation. Thus, the condition of instability of the film rupture takes the same form as that of wave generation. For simplicity, only the waves under the so-called "steady cutting" conditions (cutting speed less than 2 m/min.)[3] are considered. In the case of small film thickness, the shear force perturbation will be dominant, so Eq. (17) can be further simplified as follows:

$$h < \left(\frac{3T_i}{2\gamma k^3}\right)^{1/2} \tag{18}$$

The critical thickness for stability can be evaluated for a given wave length, if the perturbation shear stress can be calculated accordingly. Most theoretical analyses of interfacial instabilities have adopted Benjamin's quasi-laminar estimate. Benjamin's method is expected to give correct orders of the results even when it is applied to turbulent flows[12] and is used here to evaluate the scaling of the surface stress and critical film thickness for instability.

The surface stress can be evaluated as follows:[8]

$$T_i = \rho v^2 \left(\beta I/c_f\right)\alpha^3(\alpha R)^{-4/3} \tag{19}$$

$$P_r = \frac{\rho v^2 \alpha I}{R c_f} \tag{20}$$

where $\alpha = kh$ is the dimensionless wave number and $c_f$ is the friction factor. The expressions for $I$ and $\beta$ are as follows:

$$I = \int_0^\infty \left(U(y)/U_0\right) e^{-\alpha y} d(\alpha y) \tag{21}$$

$$\beta = 1.188\left(\frac{\nu_g}{\nu}\right)^{2/3}\left(\frac{\rho_g}{\rho}\right) \tag{22}$$

where $U(y)$ is the gas velocity profile that is assumed to follow the 1/7th power law,[13] $U_0$ is the streamwise gas velocity, $\nu_g$ and $\nu$ are kinematic viscosity of the gas and the melt, respectively, and $\rho_g$ is the gas density. $c_f$ can be calculated according to the following:

$$\mu\frac{V}{h} = c_f \rho_g U_0^2 \tag{23}$$

where $\mu$ is the viscosity of the melt.

The interfacial velocity can be calculated using the 1/7th power law of mean velocity profile,[13] that is:

$$\frac{U_0}{v_*} = 8.74\left(\frac{bv_*}{2\nu_g}\right)^{1/7} \tag{24}$$

$$\rho_g v_*^2 = \frac{\mu V}{h} \tag{25}$$

where $b$ is the kerf width, $\nu_g$ is the kinematic viscosity of the gas, and $v_*$ is the friction velocity. The properties of the gas phase should be taken at the local temperature.

The critical thickness below which instabilities occur is found to be approximately 5.6 x $10^{-4}$ m if the parameters in *Table 1* are used. The wave number $k$ is evaluated as $k = 2\pi f/V$, where $f$ is the striation frequency. Since it is commonly accepted that thickness of the molten layer is in the order of $10^{-5}$ m,[2,3,10] which is about one order of magnitude below the calculated critical thickness, thus the molten front is unstable and so-called slow waves will generate at the cutting front.

*Table 1*
**Physical Quantities and Parameters Used in the Simulation**

| | |
|---|---|
| $U_0$ = 340 m/s | $\mu_g$ = 4.5 x $10^{-5}$ kg/(ms) |
| $b$ = 0.4 x $10^{-3}$ m | $\rho$ = 7.8 x $10^3$ kg/m$^3$ |
| $f$ = 230 s$^{-1}$ | $\rho_g$ = 0.23 kg/m$^3$ |
| $\gamma$ = 1.0 kg/s$^2$ | $\nu$ = 0.64 x $10^{-6}$ m$^2$/s |
| $\mu$ = 5 x $10^{-3}$ kg/(ms) | $\nu_g$ = 2.25 x $10^{-4}$ m$^2$/s |

## Prediction of Striation Frequency

In the aforementioned physical model, the striation frequency is equivalent to the oscillation frequency of melt ejection and oxidation. Under high-speed cutting conditions, the frequency should be equivalent to the slow wave frequency. The wave number of the slow wave is approximately taken as the critical wave number at which the mean shear stress, $\tau$, attains the minimum value. Undamped disturbances for the liquid film of thickness, $h$, are sustained at such a minimum value. Substituted by the proper stress evaluation, Eq. (14) becomes

$$\frac{I}{c_f}\left[\frac{k\tau}{\rho} + \frac{3\beta\nu^{2/3}}{2h}\left(\frac{k\tau}{\rho}\right)^{2/3}\right] = \frac{\gamma k^2}{\rho} \tag{26}$$

Taking derivative $\partial\tau/\partial k$ of the above equation, one obtains the positive critical wave number:

$$k = \frac{I\tau}{4c_f\gamma} \tag{27}$$

The mean stress is evaluated according to

$$\tau = \mu\frac{V}{h} \tag{28}$$

Theoretical results show that the wave speed is equal to the interfacial velocity [Eq. (15)]. However, the experimental measurements show that the wave speed is actually less than the interfacial velocity. A reasonable approximation is obtained by considering a coefficient of, say, 0.8.

$$c = 0.8V \tag{29}$$

where $c$ is the wave velocity and $V$ is the interfacial velocity. This takes into account the nonlinear effects that may reduce the wave velocity. Thus, $V$ calculated from Eqs. (24) and (25) can be used to approximate wave velocity. The wave frequency is then

$$f = 0.8Vk/2\pi \tag{30}$$

As discussed in the physical model section, the wave frequency is actually the frequency of the striation. The striation wavelength is, however, a com-

bination of striation frequency and the cutting speed, $v$, as follows:

$$\lambda = v/f \tag{31}$$

The interfacial velocity, $V$, is dependent on the stationary liquid film thickness, $h$, which should be derived from steady-state energy and momentum balance. The calculation method from Vicanek et al.[2] is used to obtain the values of film thickness $h$ as a function of cutting speed and gas velocity. Vicanek et al. treated the molten front as a plane and solved the momentum equations based on boundary theory, taking the physical properties at the wall temperature instead of solving the energy equation.

**Prediction of Striation Depth**

As mentioned in the introductory section, striation formation has been found to be strongly related to oxidation in laser cutting. The exothermic oxidation typically contributes nearly half of the total energy input. The heat conduction and oxidation take the same parabolic forms as the following:

$$\frac{\partial C}{\partial t} + U(y)\frac{\partial C}{\partial x} = \frac{\partial}{\partial y}\left(D\frac{\partial C}{\partial y}\right) \tag{32}$$

$$\rho\frac{\partial c_p T}{\partial t} + \rho U(y)\frac{\partial c_p T}{\partial x} = \frac{\partial}{\partial y}\left(K\frac{\partial T}{\partial y}\right) \tag{33}$$

where $C$ is the oxygen concentration, ρ is the density, $c_p$ is the heat capacity, and $D$ and $K$ are the diffusion coefficient and heat conductivity, respectively. The hydrodynamic instability of the oxide layer described in the previous sections brings about oscillations in the oxidation process because of the large diffusivity of the oxide layer. The diffusion-controlled oxidation process can be described as follows:

$$\frac{ds}{dt} = BJ = BD\frac{\partial C}{\partial x} \tag{34}$$

where $s$ is the oxide layer thickness, $J$ is the particle current, and $B$ is a constant. If the quasi steady state approximation that the concentration on oxide surface is independent of the oxide film is valid, Eq. (34) can be written as follows:

$$\frac{ds}{dt} = BD\frac{(C_o - C_s)}{s(t)} \approx BD\frac{C_o}{s(t)} \tag{35}$$

where subscript $s$ denotes the metal-oxide interface and subscript $o$ denotes the oxide-oxygen interface. $C_s$ is near zero because of consumption of oxygen at the reaction plane. The temperature dependence of the diffusion coefficient is due to an exponential factor containing an activation energy $W$ and Boltzmann constant $k_B$.

$$D \propto \exp\left(-\frac{W}{k_B T}\right) \tag{36}$$

Note that $C_o$ is also temperature dependent,

$$C_o \propto \exp\left(-\frac{w}{k_B T}\right) \tag{37}$$

where $w$ is the internal energy. The oxidation equation can be written as follows:

$$\frac{ds}{dt} = A(p_o)\frac{\exp(-T_0\ T)}{s(t)} \tag{38}$$

where $A$ is a coefficient that has presumably a linear relationship with the oxygen pressure $p_o$ at the surface of the molten front. $T_0$ is the activation temperature for the diffusion. An estimate for $s$ can be achieved by neglecting temperature variation and simply integrating Eq. (38) to give the well-known parabolic equation:

$$s_m{}^2 = A(p_o)t_p \tag{39}$$

where $s_m$ is the maximum thickness of the oxide layer. The time period $t_p$ is the inverse of frequency from Eq. (30). If one calculates the striation frequency from Eq. (30), the maximum depth of the striations can be estimated from Eq. (39) if the coefficient is experimentally calibrated.

The above approximation assumes that the oxide layer is directly related to the striation depth. Striation formation is a complicated phenomenon, and simplifications are needed for modeling and simulation efforts to obtain quantitative results. Another simplified yet reasonable approach to predict striation depth is to relate the striation depth to the temperature fluctuation range of the molten front. Experimental studies have confirmed that the striation pattern can be correlated to the temperature fluctuation.[5] A numerical simulation has been car-

ried out to simulate the front temperature fluctuation, where parabolic growth of the oxide layer is assumed, followed by removal due to hydrodynamic instability.[14] The period of this growth-removal cycle is given from the frequency prediction described before. The striation depth can be calibrated from the simulated temperature fluctuation range.

## Calculation and Experimental Results

### Striation Frequency

For a given laser power, the striation frequency is related to the surface velocity [Eqs. (24) and (25)] and wave number [Eq. (27)], which in turn depends on the gas velocity and liquid film thickness. The gas velocity is dependent on the gas pressure as well as the interaction of the gas jet with the workpiece. The average values of the streamwise gas velocity are obtained from numerical simulations carried out by the same authors. The details of the numerical simulation of the gas effects will be presented in the other paper. The liquid film thickness is dependent on the gas velocity and the cutting speed.

Experiments were carried out for oxygen-assisted cutting of 1.6 mm thick steel 1018 with a $CO_2$ laser (*Table 2*). The laser was operated in continuous wave mode with focal length of 2.5 in. The laser beam was focused on the material surface. The gas delivery nozzle is a convergent nozzle with diameter 1.35 mm and standoff 1.0 mm. For Group 1 experiments, the gas pressure is held at 2.1 bar (30 psi, measured on gauge) and the cutting speed is varied from 15 mm/s to 50 mm/s. In Group 2 experiments, the cutting speed is fixed at 30 mm/s and the gas pressure is varied from 0.8 to 3.8 bar (measured on gauge). The striation wavelength and depth are obtained from Talysurf profiles taken from a position 0.5 mm from the top of the cut edge.

*Figures 6* and *7* show the calculated liquid film thickness and interfacial velocity against the cutting speed, corresponding to the experimental parameters. The wave number calculated from Eq. (28) is virtually unaltered with changes of the cutting speed. The corresponding wavelength of slow waves is about 1.56 mm if a typical value of $I = 0.30$ in Eq. (21) is chosen.

*Table 2*
**Experimental Conditions**

| Section Thickness | Power | Group 1 | Group 2 |
|---|---|---|---|
| 1.6 mm | 500 W | Gas pressure 2.1 bar | Cut speed 30 mm/s |
| | | Cut speed 15-50 mm/s | Gas pressure 0.8-3.8 bar |

The predicted striation wavelength and the experimental results are given in *Figure 8*, and they are in agreement. The increase in cutting speed causes the liquid film thickness and thus the interfacial velocity to increase. As a result, the striation frequency increases, but not as much as the increase of the cutting speed. The net result, therefore, is that the striation wavelength increases with the cutting speed.

For convergent nozzles, when the stagnant gas pressure is higher than 0.89 bar (measured on gauge), that is, when the ambient pressure is lower than the critical pressure (0.528 of stagnant gas pressure), the gas jet cannot expand normally. The gas pressure at the nozzle exit will be held at the critical pressure (choked flow) and the velocity is equivalent to the sound velocity at the local temperature. Immediately after the nozzle exit, there is a system of shockwaves beginning at the nozzle edge.[15] However, the numerical simulation shows that the main stream gas velocity remains relatively constant inside the cut kerf (between 1.0 mm and 2.5 mm in *Figure 9*) despite the increasing gas pressure. Consequently, the wave velocity will not change much, and the striation frequency is almost independent of the gas pressure. *Figure 10* shows the measured and predicted striation wavelengths against the gas pressure. The wavelength does not change much when the gas pressure is higher than 0.89 bar.

### Striation Depth

Striation depth is evaluated using Eq. (39). This assumes that the parabolic growth of the oxide layer is directly related to the striation depth. *Figure 11* shows the predicted maximum striation depth against the experimental measurements. The coefficient in Eq. (39) is calibrated to be a constant of $4 \times 10^{-8}$. The increase of the striation frequency with the cutting speed gives a shorter interaction period for the oxidation and melting process and thus reduces the striation depth. The prediction is consistent with the experimental results.

*Figure 12* shows the maximum striation depth against the gas pressure. The $p_o$ in Eq. (39) is the stagnant pressure on the cut edge, which is nearly proportional to the total pressure at the nozzle exit. The pressure on the cut edge increases as the gas

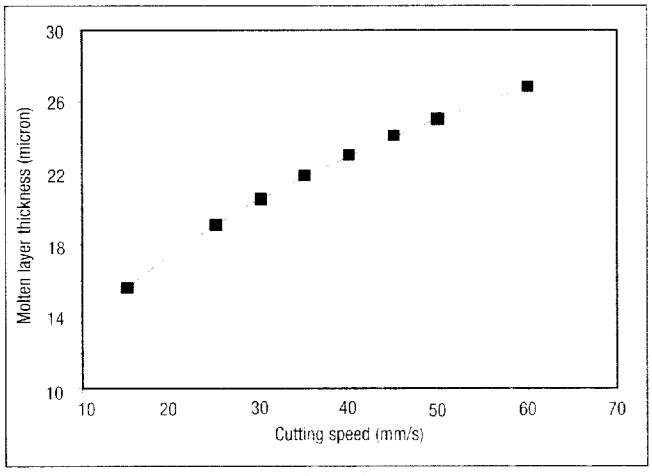


*Figure 6*
**Calculated Liquid Film Thickness vs. Cutting Speed**

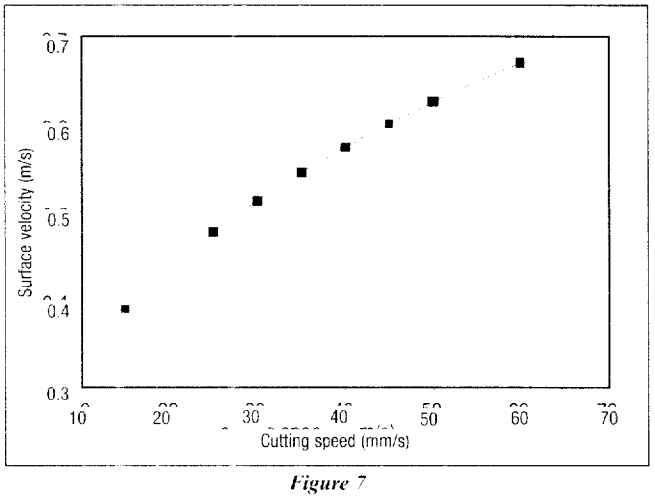


*Figure 7*
**Calculated Interfacial Velocity vs. Cutting Speed**

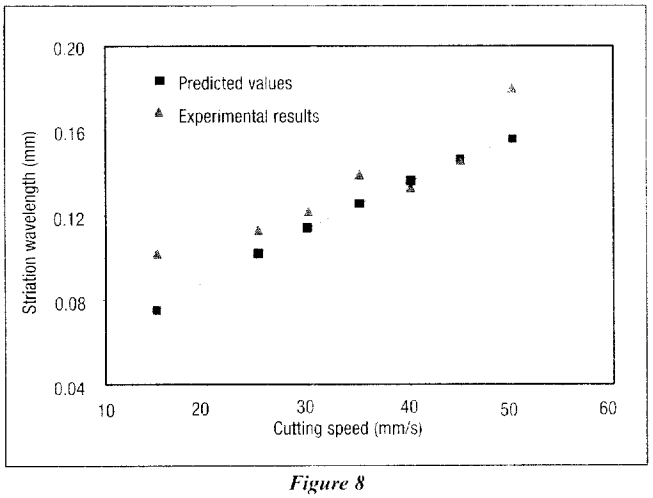


*Figure 8*
**Striation Wavelength vs. Cutting Speed**

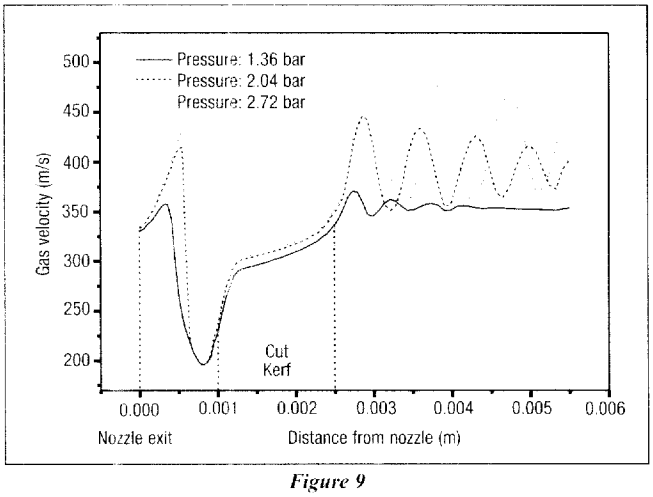


*Figure 9*
**Streamwise Gas Velocity from Nozzle**

pressure increases, resulting in higher oxygen concentrations on the cut edge, which is beneficial for oxidation. Thus, the striation depth increases.

Based on this molten layer instability analysis, the transient temperature fluctuation is captured numerically. The details of the numerical simulation process are described in Chen, Yao, and Modi.[14] The relevant results are summarized here. *Figure 13* shows calculated front temperature fluctuation under a typical condition. Since the coefficient of the parabolic growth is not readily available, it is calibrated so that the temperature fluctuation is around a level known from experiments. When the oxide layer starts to grow, the oxidation slows down because of the high resistance of the oxide layer to the oxygen diffusion, and thus the temperature starts to drop. Once the oxide layer is removed, the temperature quickly picks up due to a sudden increase of oxygen flux and reaction energy. *Figures 14* and *15* show the calculated temperature fluctuation range and the measured striation depth for different cutting speeds and gas pressures, respectively. As seen, the decrease of the temperature fluctuation range corresponds to the decrease of the striation depth for increasing cutting speed, and the opposite trends hold for increasing gas pressure.

## Discussions

It is interesting to note that when thick sections are cut, there are two striation patterns produced on cut edges, with the primary striation pattern on the top and another more irregular pattern on the bottom. This is understandable if there are two waves present on the cut edge, one followed by another. It is known that the transition to two striation patterns occurs when the workpiece thickness is above 1.5 mm to 2.0 mm. This is close to the calculated value

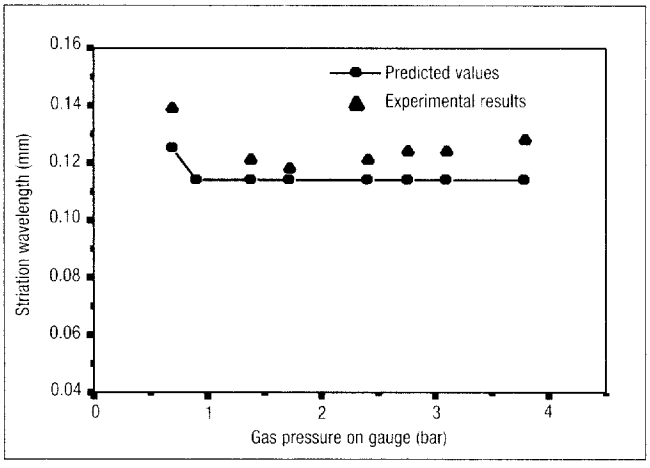


*Figure 10*
**Striation Wavelength vs. Gas Pressure**

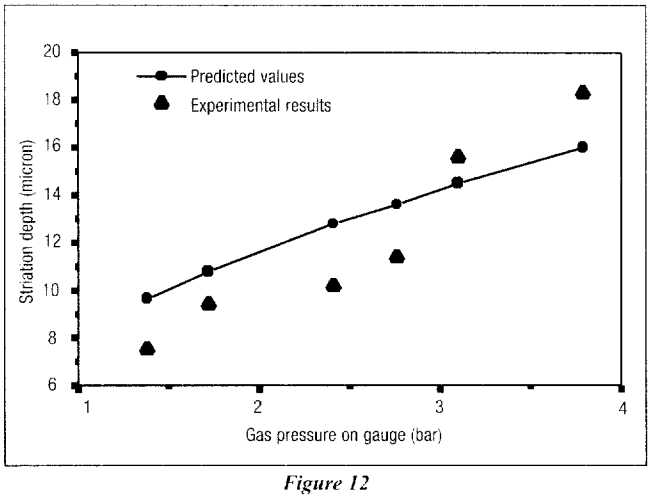


*Figure 12*
**Maximum Striation Depth vs. Gas Pressure**

of wavelength. When waves travel downward, the wave velocities become irregular, causing relative irregularity of the secondary striation pattern commonly observed. This topic is intended to be investigated in the future work.

In the current prediction of striation wavelength, the physical properties of gas and liquid phase are assumed to be constant. The approximation is valid only when the energy balance does not change significantly as the cutting speed or the gas pressure varies. A more accurate model would incorporate the energy balance into the calculations. Since the oxidation process in laser cutting is far from being well understood and the relationship between the molten layer and the oxidation layer is not clear, approximations were made, and the calculations have to be calibrated to evaluate the striation depth. The molten front is simplified to be two-dimensional, of uniform thickness. The actual profile of the

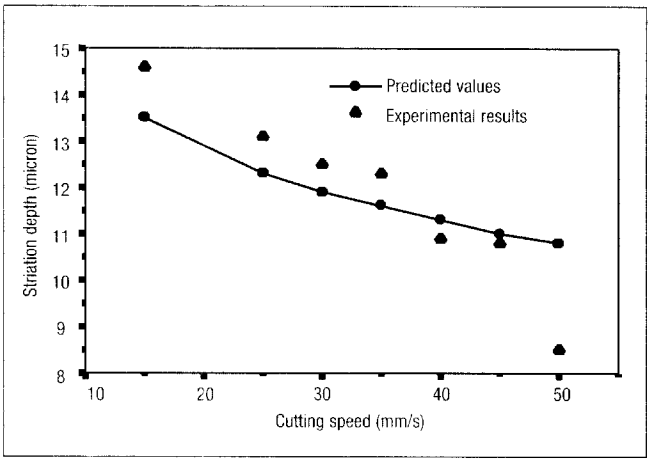


*Figure 11*
**Maximum Striation Depth vs. Cutting Speed**

molten front is, however, curved, and the thickness increases from top to bottom. A slow wave on the molten front may consist of a band of wave numbers, and the wave numbers may be away from the critical wave number.

There are other effects that may influence the instabilities of the thin liquid film. There are shock waves in the gas jet after the nozzle exit, and the gas jet becomes turbulent because the reservoir pressure for laser cutting is usually higher than 0.89 bar of gauge pressure. The turbulent fluctuation of the airflow will increase the surface stresses produced by interaction of the mean airflow, making the liquid film more unstable. The viscosity and the surface tension of the liquid phase generally have stabilizing effects on the liquid film. In oxidation cutting, the viscosity and the surface tension of the iron oxide are lower than those of pure molten iron, which increases the instability of the molten front.

## Conclusions

A theory of the unstable characteristic of the melt ejection combined with the oxidation oscillation is proposed to explain the mechanism of striation generation. When the cutting speed is small, the liquid film ruptures on the cutting front. When the cutting speed increases to some point, waves are produced on the top of the cutting front in place of film rupture. Each wave crest or film rupture results in a sudden increase of the melt removal and thus the acceleration of the oxidation and the melting. As a result, a cyclic pattern is formed on the cut edge. The striation frequency is related to the frequency of the slow waves or film rupture. The calculated striation fre-

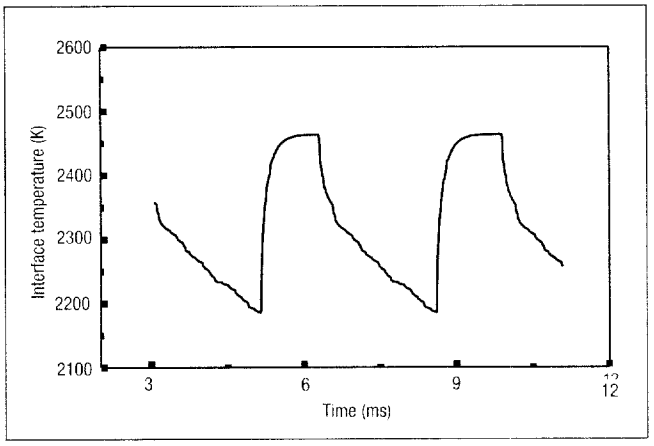


*Figure 13*
**Temperature Fluctuation at the Oxygen-Melt Interface**

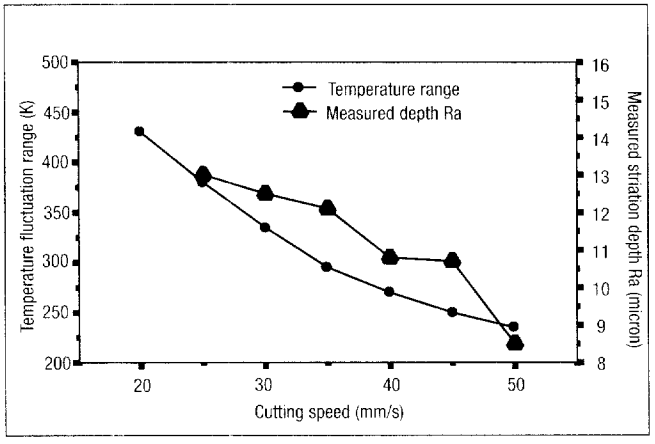


*Figure 14*
**Temperature Fluctuation Range and Measured Striation Depth vs. Cutting Speed**

quency (or wavelength) matches the experimental results. The maximum depth of the striation pattern is predicted along with the temperature fluctuation range at the molten front, and they show similar trends. The predicted tendencies are consistent with the experimental results.

## Acknowledgment

This work is supported in part by an NSF grant (DMI-9500181). Assistance by Dr. W. Li during the experiments is also gratefully acknowledged.

## References

**1.** D. Schuocker, "Dynamic Phenomena in Laser Cutting and Cut Quality," *Applied Physics B: Lasers and Optics* (v40, 1986), pp9-14.
**2.** M. Vicanek et al., "Hydrodynamic Instability of Melt Flow in Laser Cutting," *Journal of Physics D: Applied Physics* (v20, 1986), pp140-145.
**3.** Y. Arata et al., "Dynamic Behavior in Laser Gas Cutting of Mild Steel," *Trans. JWRI* (v8, n2, 1979), pp15-26.
**4.** A. Ivarson et al., "The Oxidation Dynamics of Laser Cutting of Mild Steel and the Generation of Striations on the Cut Edge," *Journal of Materials Processing Technology* (v40, 1994), pp359-374.
**5.** P. Di Pietro, Y.L. Yao, and K. Chen, "An Experimental Study of On-Line Estimation of Striations in Laser Cutting Process," *Technical Papers of NAMRI/SME* (Dearborn, MI: Society of Manufacturing Engineers, 1997), pp105-110.
**6.** T.J. Hanratty, "Interfacial Instabilities Caused by Air Flow," *Waves on Fluid Interfaces*, R.E. Meyer, ed. (New York: Academic Press, 1983).
**7.** S.P. Lin, "Film Waves," *Waves on Fluid Interfaces*, R.E. Meyer, ed. (New York: Academic Press, 1983).
**8.** A.D.D. Craik, "Wind-Generated Waves in Thin Liquid Films," *Journal of Fluid Mechanics* (v26, 1966), pp269-392.
**9.** S.G. Yaintsios and B.G. Higgins, "Rupture of Thin Film: Nonlinear Stability Analysis," *Journal of Colloid and Interface Science* (v147, n2, 1991), pp341-351.
**10.** N.K. Makashev, "Gas-Hydro-Dynamics of CW Laser Cutting of Metals in Inert Gas," *Proc.* of SPIE, Industrial Lasers and Laser Material Processing (v2257, 1993), pp2-9.
**11.** C.C. Lin, *The Theory of Hydrodynamic Stability* (Cambridge, UK: Cambridge Univ. Press, 1955).
**12.** T.B. Benjamin, "Shearing Flow Over a Wavy Boundary," *Journal of Fluid Mechanics* (v6, 1959), pp161-205.
**13.** H. Schlichting, *Boundary-Layer Theory* (New York: McGraw-Hill, 1979).
**14.** K. Chen, Y.L. Yao, and V. Modi, "Numerical Simulation of Oxidation Effects in Laser Cutting of Mild Steels," ICALEO'97, Laser Institute of America (v83, Sec. B 37-45, 1997).

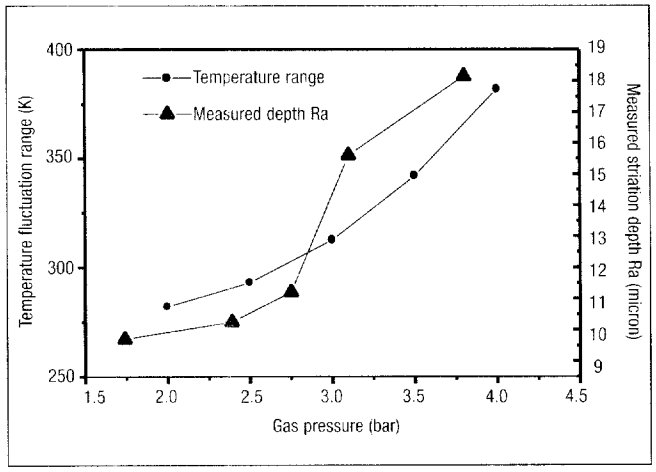


*Figure 15*
**Temperature Fluctuation Range and Measured Striation Depth vs. Gas Pressure**

**15.** J. Fieret, "Overview of Flow Dynamics in Gas-Assisted Laser Cutting," *Proc.* of SPIE, High Power Lasers (v801, 1987), pp243-250.

## Authors' Biographies

Kai Chen is currently a PhD candidate in the Department of Mechanical Engineering at Columbia University. He received his master's degree from Dartmouth College and bachelor's degree from Tsinghua University (China). He is currently working toward a doctoral degree in the Manufacturing Research Laboratory at Columbia. His dissertation topic concentrates on numerical and experimental investigation of laser machining, including the studies of striation formation, oxidation, gas effects, and pulsed laser machining.

Y. Lawrence Yao is an associate professor in the Department of Mechanical Engineering at Columbia University. He received his BE degree in mechanical engineering from Shanghai Jong Tong University (China) in 1982 and his MS and PhD degrees in mechanical engineering from the University of Wisconsin-Madison in 1984 and 1988, respectively. Prior to joining Columbia in 1994, Dr. Yao was a senior lecturer in the School of Mechanical and Manufacturing Engineering at the University of New South Wales (Australia). His areas of research interest include laser materials processing, industrial manipulators in manufacturing, and monitoring and diagnostics of manufacturing processes. His current activities have been focused on experimental and numerical investigations of issues involved in laser machining, laser micromachining, and laser forming. Striation formation mechanism, oxygen effects, gas jet and workpiece interactions, and residual stress and strain rate effects are among the topics under investigation.